Visual Neuroscience

www.cambridge.org/vns

Classification of pseudocalcium visual responses from mouse retinal ganglion cells

H. Shabani[1], Mahdi Sadeghi[1], E. Zrenner[1,2], D.L. Rathbun[1,3] and Z. Hosseinzadeh[4]

[1]Institute for Ophthalmic Research, Centre for Ophthalmology, Eberhard Karls University, Tübingen, Germany, [2]Werner Reichardt Centre for Integrative Neuroscience (CIN), Tübingen, Germany, [3]Department of Ophthalmology, Detroit Institute of Ophthalmology, Henry Ford Health System, Detroit, Michigan, and [4]Department of Molecular and Cellular Mechanisms of Neurodegeneration, Paul Flechsig Institute for Brain Research, University of Leipzig, Leipzig, Germany

Research Article

Cite this article: Shabani, H., Sadeghi, M., Zrenner, E., Rathbun, D.L. & Hosseinzadeh, Z. (2021). Classification of pseudocalcium visual responses from mouse retinal ganglion cells. *Visual Neuroscience* 38:E016
https://doi.org/10.1017/S0952523821000158

Received: 30 April 2021
Revised: 08 September 2021
Accepted: 14 September 2021

Keywords:
pseudocalcium; calcium kernel; calcium trace; chirp

Corresponding author:
D.L. Rathbun,
e-mail: drathbu2@hfhs.org;
Z. Hosseinzadeh,
e-mail: Zohreh.Hosseinzadeh@medizin.uni-leipzig.de

This is an updated version of the original article. For details please see the notice at https://doi.org/10.1017/S0952523822000037.

Abstract

Recently, a detailed catalog of 32 retinal ganglion cell (RGC) visual response patterns in mouse has emerged. However, the 10,000 samples required for this catalog—based on fluorescent signals from a calcium indicator dye—are much harder to acquire from the extracellular spike train recordings underlying our bionic vision research. Therefore, we sought to convert spike trains into pseudocalcium signals so that our data could be directly matched to the 32 predefined, calcium signal-based groups. A microelectrode array (MEA) was used to record spike trains from mouse RGCs of 29 retinas. Visual stimuli were adapted from the Baden et al. study; including moving bars, full-field contrast and temporal frequency chirps, and black–white and UV-green color flashes. Spike train histograms were converted into pseudocalcium traces with an OGB-1 convolution kernel. Response features were extracted using sparse principal components analysis to match each RGC to one of the 32 RGC groups. These responses mapped onto of the 32 previously described groups; however, some of the groups remained unmatched. Thus, adaptation of the Baden et al. methodology for MEA recordings of spike trains instead of calcium recordings was partially successful. Different classification methods, however, will be needed to define clear RGC groups from MEA data for our bionic vision research. Nevertheless, others may pursue a pseudocalcium approach to reconcile spike trains with calcium signals. This work will help to guide them on the limitations and potential pitfalls of such an approach.

Introduction

In efforts to restore sight to the blind through electrical stimulation of the retina, termed bionic vision (Zrenner, 2002; Demchinsky et al., 2019; Ayton et al., 2020), the nonspecificity of electrical stimulation remains an unresolved problem (Rathbun et al., 2018). While we have known for decades that standard electrical stimulation indiscriminately activates the different retinal ganglion cell (RGC) types, only recently has it even been possible to discriminate between the full range of these many functionally distinct types. In 2016, Baden et al. published a landmark work describing 32 distinct RGC *groups* in the mouse retina. These groups serve as reasonable stand-ins for the true *types* that are believed to make up the neural code of the retina. Subsequent physiologic and molecular work has converged around the likelihood that there are at least 30 and possibly up to 50 mouse RGC types, with the complete count unlikely to fall outside of this range: 47 morphological types (Bae et al., 2018), 40 genetic types (Rheaume et al., 2018), 28 physiological types using spike distance (Jouty et al., 2018), and 45 types, scRNA-seq (Tran et al., 2019). Therefore, with the full catalog of mouse RGC types at hand, it is finally possible to investigate how each one responds to electrical stimulation, in the hopes of discovering strategies for type-specific electrical stimulation in bionic vision devices (Hosseinzadeh et al., 2019).

Historically visual classification of RGC types has lagged behind morphological classification (Boycott & Wässle, 1974; Perry & Cowey, 1984). Early work characterized ON- and OFF-center RGCs responding to light increases and decreases, respectively (Kuffler, 1953). Later Enroth-Cugell and Robson (1966) showed in cats how linear X cells and nonlinear Y cells differentially respond to sinusoidal gratings. Barlow et al. introduced four additional types of ON–OFF directionally selective ganglion cells in rabbits (Barlow et al., 1964; Barlow & Levick, 1965). Many other type definitions have since been articulated, however, most work has only focused on a few of them at a time.

An early attempt at statistically driven functional classification that combined these and other classification schema was only able to identify five different RGC groupings (Carcieri et al., 2003); whereas subsequent, more sophisticated methods yielded 12 groups (Farrow & Masland,

© The Author(s), 2021. Published by Cambridge University Press.

2011). Still, these 12 groups barely rivaled the 15 or so morphological types proposed at the time (Wässle, 2004). Finally, in 2016, a leap was made to 32 functionally distinct groups (Baden et al., 2016). Importantly, the estimated coverage factor for these 32 groups indicated that only a few additional groups were likely to remain unidentified.

The RGC group catalog of Baden et al. (2016) based on visual function was possible because two-photon calcium imaging could be used as a high-throughput method to record visual responses from 10,000 cells in a reasonable amount of time (Grienberger & Konnerth, 2012). Unfortunately, calcium imaging is not yet optimal for *ex vivo* retinal electrostimulation experiments due to technical limitations including electrode damage caused by the imaging lasers, nonremovable artifacts, and saturation of microelectrode array (MEA) recording amplifiers (Shew et al., 2010). Therefore, we sought to benchmark our data, collected with a MEA, to the Baden et al. group's by converting extracellularly recorded spike train data into pseudocalcium traces. Thus, we could use calcium trace-based definitions from the dataset they published to classify each of our individual responses—without the burden of collecting our own set of 10,000 responses.

In matching our data to the catalog of Baden et al. with pseudocalcium traces, we have met with only partial success—which we detail here. Although our efforts to sort mouse RGC spike trains into 32 groups remain incomplete, we believe that others may benefit from the present description of those efforts and discussion of the fundamental limitations underlying them.

Materials and methods

C57BL/6 mice were housed under standard white cyclic lighting and had free access to food and water. All procedures were in accordance with the ARVO statement for the use of animals in ophthalmic and visual research, and approved by the Tübingen University committee on animal protection.

Experimental rig

We used a 60-channel MEA to record extracellular voltage signals from RGCs. As detailed in previous studies (Hosseinzadeh et al., 2017; Jalligampala et al., 2017) we anesthetized the mice with isoflurane and then killed them by cervical dislocation before isolating retinal tissue from the pigment epithelium, sclera, and other tissues of the eye. Retinas were kept in a carbogenated (95% O_2, 5% CO_2) artificial cerebrospinal fluid. Appropriate conditions in terms of pH, oxygenation, temperature and nutritional requirements were ensured *via* a pump continuously perfusing the tissue with this artificial medium. The retinas were then laid on the MEA (Multichannel Systems, Reutlingen, Germany) with their ganglion cell layer facing downward. A dialysis membrane on a Teflon ring was placed on top of the tissue to optimize electrical contact by applying gentle pressure.

Recording system

The electrical signals detected by the MEA (200 μm electrode spacing and 30 μm electrode diameter) were recorded using a Windows XP computer equipped with Multichannel Systems hardware and software including the MEA60 system, RS-232 interface, a 60-channel preamplifier with integrated filters and a blanking circuit, main amplifier, MC_Card data acquisition hardware, and an analog input card to record stimulus timing signals. Data was sampled at the highest possible rate of 50 kHz/channel and collected using MC_Rack.

Offline data processing, analysis

Our data processing protocol involved filtering, spike detection, and spike sorting. These steps were automated and conducted on a dedicated server using commercial software (Offline Sorter, Plexon Inc., Dallas, TX). Manual inspection minimized Type I and Type II errors in spike sorting and identified the ideal solution. Sorted spike times and accompanying stimulus time stamps were then collected with NeuroExplorer (Plexon Inc., Dallas, TX) and exported to MATLAB 2018b (The Mathworks, Natick, MA) for subsequent analysis with a suite of custom scripts.

Pseudocalcium traces

Key to this study was the conversion of the time varying spike rate into a pseudocalcium trace. In order to convert spiking activity to pseudocalcium traces we used an Oregon Green BAPTA-1 (OGB) kernel provided by Baden et al. (2016). This kernel was estimated from the average of calcium events triggered by single spikes in response to full-field flash stimulation for multiple RGCs.

Visual stimulation

For light stimulation, we focused a developer module projector (DLP® LightCrafter 4500, Texas Instruments, Dallas, TX) through a custom light path of lens, mirror, and condenser onto the MEA. Stimulator intensity (as photoisomerization rate, P*/s/cone) was calibrated to match the previous Baden et al. (2016) study as closely as possible, with the white stimulus set to 3×10^4 P*/s/cone photoisomerization rate for mouse UV- and M-cones and the black stimulus set to 10^4 P*/s/cone. A steady mean illumination 2×10^4 P*/s/cone was present during, before, and after all electrical and visual stimuli to maintain adaptation state. Light stimuli included: full-field flash 2 s ON (white) and 2 s OFF (black); a chirp stimulus consisting of two sinusoidal intensity modulations (Fig. 2a), one with increasing frequency and one with increasing contrast; drifting 1000 × 300 μm bars with vertical bars at 15 locations, horizontal bars at 10 locations, and diagonal bars at 17 location for each diagonal axis, with the centers of adjacent bars separated by 200 μm; and full-field color flashes for 3 s each in a sequence of blue, black, green, and black.

Visual classification

In the reference study, algorithmic clustering was augmented with a few additional interventions that were not possible here. First, cells were originally separated based on direction selectivity to drifting bar stimuli. However, despite our best attempts at both replicating previous analysis and applying novel analyses we could not satisfactorily differentiate direction and orientation selective cells based on responses to our stimulus (see section "Discussion"). Nevertheless, we were still able to match cells from our dataset to each of the DS and OS clusters of the original report based solely on responses to the other stimuli. Second, alpha cells were originally discriminated based on soma size. Because we did not have imaging data for our recorded cells, we were unable to flag alpha cells in this way (clusters 6–8, 11–13, 33, and 34; see Fig. 3), although we were still able to use visual stimuli to match some alpha cells (clusters 11, 33, and 34). Third, because it can be difficult to discriminate amacrine

https://doi.org/10.1017/S0952523821000158 Published online by Cambridge University Press

cell (AC) and ganglion cell somas in calcium imaging, immunohistochemistry was used in the previous study to identify AC clusters. It is unlikely that we recorded spiking responses from ACs, but because this remains a slim possibility—despite their reputation as nonspiking cells—we matched our dataset to the full set of 75 cluster definitions including 26 AC clusters, as well as a 76th cluster for noisy cells. Few of our cells were best matched with an AC cluster with one exception noted in *Results*.

As previously reported (Baden et al., 2016), many individual RGC recordings were not sufficiently driven by the stimulus to support robust classification. Accordingly, we estimated how strongly the responses were driven by the stimulus by dividing the response variance across trials by the overall variance of responses. Spike counts were binned at 100 ms, response variance for each bin was calculated across at least 10 trials, and these values were then averaged. The overall variance was calculated across the full set of time bins and trials including both response intervals and spontaneous intervals. Cells with a response variance higher than the overall variance (a ratio higher than 1) were excluded from analysis as unreliably driven cells.

Finally, we projected the pseudocalcium traces of our visually responsive cells onto the lower-dimensional feature space previously determined by Baden et al. using sparse principal components analysis (sPCA). By using the sPCA features of the previous study, we ensured that our data was analyzed according to their definitions for cell clusters. We refer the reader to the earlier Baden et al. (2016) study for more extensive details on feature selection and clustering. These sPCA features included 20 features from the chirp, 8 features from the moving bar, 4 features from its temporal derivative, and 6 features from the color stimulus, yielding a 38-dimensional feature vector for each cell. Two features from a visual noise stimulus were excluded because very few of our cells produced significant receptive field maps in response to this stimulus. Classification was performed by calculating the Euclidean distance between the feature vector of each cell and the average feature vector of each cluster of reference dataset cells, assigning each cell to the most similar reference cluster.

Electrical stimulation

To calculate and examine the spike triggered average (STA) electrical preference of each cell group, we presented an electrical Gaussian noise stimulus with a mean of −800 mV and s.d. of 35% (280 mV) developed by Sekhar et al. (2016). The duration of each pulse was set to 1 ms and the stimulation frequency was 25 Hz. The length of each trial of noise stimulation was 100 s; and from experiment to experiment the number of repetitions varied from 15 to 30. A stimulus generator (STG4000 Series; MCS, Reutlingen, Germany) was used for electrical stimulation. A LNP fitting toolbox (https://github.com/pillowlab/LNPfitting) (Williamson et al., 2015) was used to compute the STA of burst-corrected responses (Rathbun et al., 2018) for each RGC. The STA can also be viewed as an estimate of the filter applied by the neuron to incoming stimuli —the electrical input filter.

Results

The intent of this study was to assess the possibility of assigning RGCs to predefined, putative types by converting their binary spiking data to pseudocalcium traces. Having assigned RGCs by type we hoped to then evaluate the electrical input filter (STA) of each type for use in retinal prosthetics.

We recorded the spiking responses of 892 mouse RGCs from nine retinas. For a stimulus-driven cell, the response variance should be lower than the overall variance, yielding a variance ratio less than 1. All cells with a variance ratio of 1 or higher were excluded, leaving 653 RGCs for classification.

Estimating calcium traces from spiking data

To convert our binary spiking data into pseudocalcium traces, each spike was convolved with the OGB kernel. Initially, we found that our traces were categorically more transient than those reported in Baden et al. We eventually realized that this strong discrepancy is the result of subthreshold calcium signals that are present in calcium imaging data but cannot be recorded in extracellular spiking data (Discussion). Reasoning that stimulus-driven spikes and subthreshold signals are strongly correlated, we doubled the duration of the OGB kernel as an imperfect but effective compensatory measure. This yielded a range of pseudocalcium response patterns much more similar to the reference calcium data. Fig. 1 shows an example of this conversion for a sample recording of flash stimulation responses. After comparing the classification results for both kernels, the doubled kernel was found to distribute data more broadly amongst the available groups rather than restricting assignment to only the most transient response groups. Therefore, this kernel was used for final clustering.

Classification

After converting binary spiking data to pseudocalcium traces, they were normalized similar to Baden et al. and each cell's median across different trials was used (Fig. 2). Median traces were projected into a predefined feature space; and each cell was assigned to its most similar cluster. In the original study, responses were sorted into 75 distinct clusters. Clusters 1–39 were definitely RGCs; 40–49 were suspected RGCs; and 50–75 were ACs. For our analysis, one last cluster, number 76, contained all cells from the original study with noisy responses. Some of our data were best matched to this cluster and were subsequently disregarded. In the original study, sometimes multiple clusters were found to be subsets of distinct RGC groups and were therefore grouped together. Thus, the 49 RGC *clusters* yielded 32 distinct RGC *groups*. It was these 32 groups that we sought to assign to our new dataset through matching of the underlying clusters—as they represent an, admittedly provisional, scheme for classifying RGCs according to true physiological type. Fig. 3 shows the cluster means from the benchmark dataset (*left column*) as well as pseudocalcium means for our classified RGCs (*middle and right*). Our original experiments for pseudocalcium classification yielded 892 RGCs from nine retinas (Fig. 3, middle). In a follow-up experiment we used similar methods and were therefore able to increase this dataset to 2303 RGCs from 29 retinas (Fig. 3, right).

We found that 2303 stimulus-driven RGCs recorded from 29 retinas sorted into 29 of the 39 previously reported "certain" RGC clusters. Our RGCs also matched with 5 of the 10 "suspected" RGC clusters. Thus, 34 of the 49 RGC clusters (70%) were matched by our data. Clusters 76 (noisy responses) and 50–75 (displaced ACs) were omitted from the figure for clarity. When the 49 RGC clusters were merged to yield 32 functionally distinct RGC groups, our data was found to match 27 of the 32 groups (84%). Therefore, while we were able to assign cells from our recordings to most

https://doi.org/10.1017/S0952523821000158 Published online by Cambridge University Press

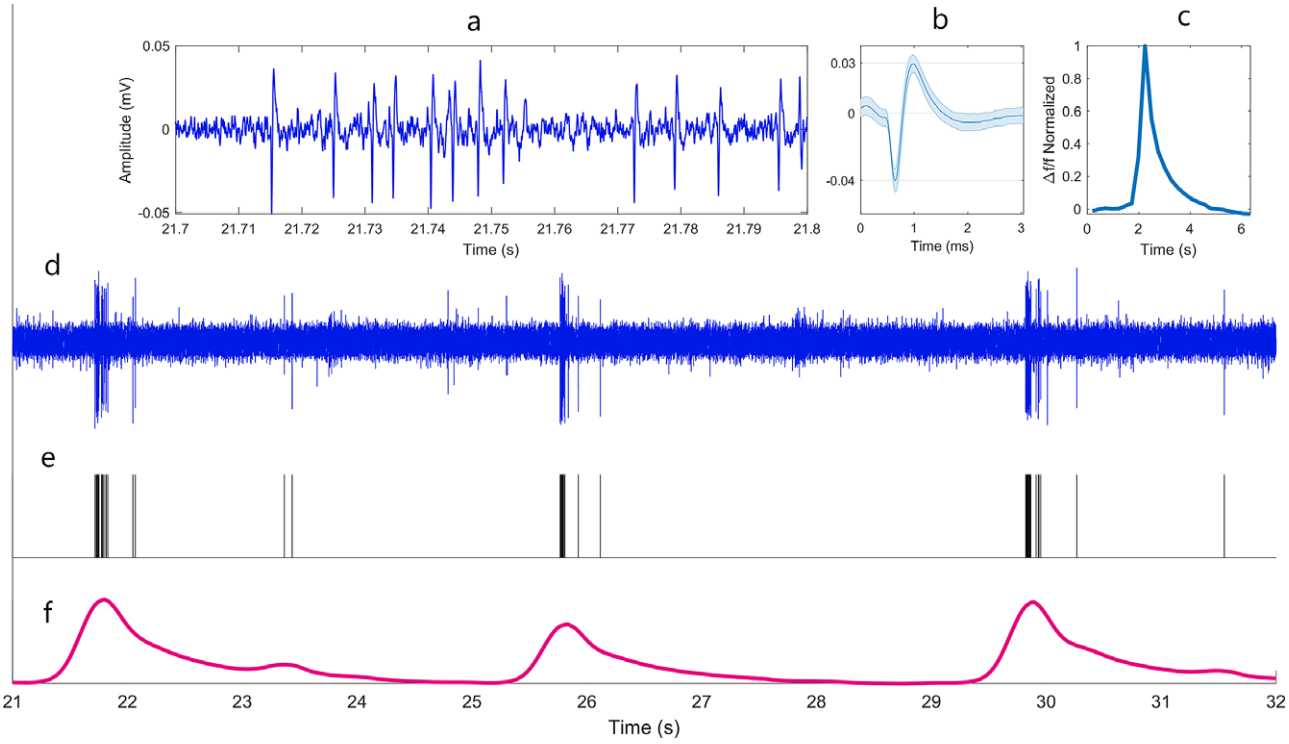


Fig. 1. Sample raw data and equivalent pseudocalcium trace. (**a**) 100 ms of filtered voltage recording excerpted from (**d**). (**b**) Average of extracellular action potentials (mean ± s.d.). Dashed lines highlight baseline and peak. (**c**) OGB kernel. (**d**) 11 s sample of filtered data from an ON cell in response to the cycling flash stimulus. (**e**) Rastergram of spike times for this cell (note excluded spikes around 25 s assigned to a different cell). (**f**) Pseudocalcium trace produced by convolving the rastergram (**e**) with the OGB kernel (**c**).

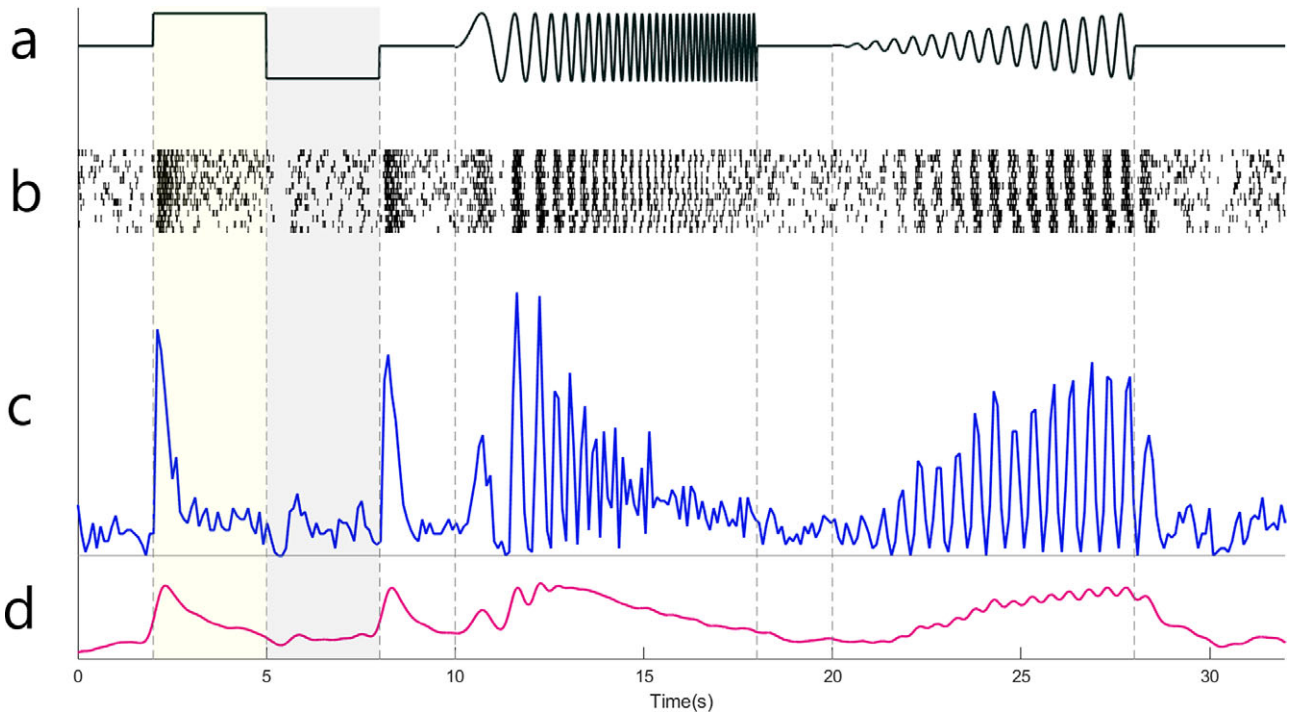


Fig. 2. Pseudocalcium trace generation for the chirp stimulus. (**a**) Stimulus brightness over time including 3 s ON and 3 s OFF full-field flash; gray, and two "chirps" composed of increasing frequency and increasing contrast respectively. (Vertical dashed lines separate various stimuli as well as the mean gray background). (**b**) Raster of spike times across multiple repetitions of the stimulus. (**c**) Peri-stimulus time histogram (PSTH) of these spike times across all trials using 100 ms time bins. (**d**) Pseudocalcium trace generated by convolving the rastergrams with the OGB kernel and averaging across trials.

https://doi.org/10.1017/S0952523821000158 Published online by Cambridge University Press

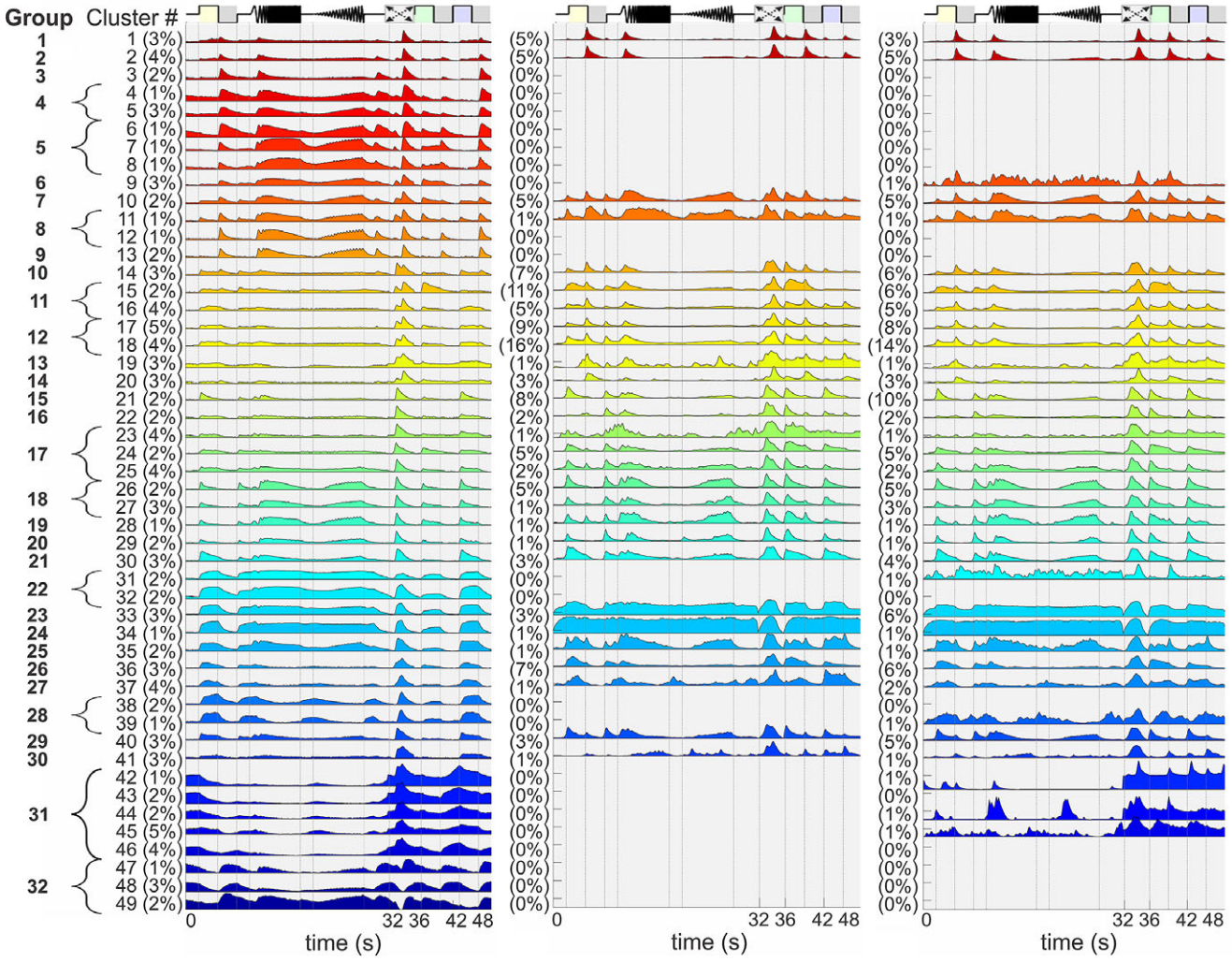


Fig. 3. Average time varying calcium signals for the 49 RGC *clusters* reported in Baden et al. (2016) (*left*) average pseudocalcium signals for the spiking data assigned to these clusters from our present dataset (*middle*), and from an expanded dataset (*right*). Each trace was normalized to its respective peak. Value at left of each cluster is the percent of RGCs assigned to each cluster, rounded up. Clusters were combined to produce the 32 distinct RGC *groups* (indicated at far left), and loosely organized with OFF cells near the top, ON–OFF cells in the middle, and ON cells at the bottom. Vertical dashed lines separate stimuli from one another and from baseline responses to the mean gray background stimulus. The segments in order were: gray, white (ON), black (OFF), gray, frequency chirp, gray, contrast chirp, gray (and black), drifting bar, green, black, blue, and black.

previously reported groups, some specific groups were not matched by our data (Discussion). Importantly, the mean cluster responses identified for 9 retinas remain largely the same as for 29 retinas. Each of the four new clusters constitutes only 1% or less of the dataset, resulting in noisy and unreliable cluster means. Overall, this indicates that these clusters are unlikely to change much with an increased dataset.

Estimating electrical input filters

Previous work has shown that electrical input filter shapes vary according to coarsely defined RGC type (Sekhar et al., 2017; Ho et al., 2018). Our goal in developing the present classification method was to examine nuanced distinctions between input filters (STAs) for the 32 different RGC groups. Fig. 4 shows cluster averages for all 792 RGCs from the larger dataset that had a statistically significant STA (as defined in Sekhar et al., 2016). In agreement with our previous work (Sekhar et al., 2017), OFF clusters as defined in the Baden study (1, 2, 10, and 11) have downward deflections directly to the left of time zero in their electrical STAs. Likewise, most ON clusters (21, 22, 24–31, 33, 35, and 40) have upward deflections; although clusters 23 and 37 are downward and 34, 36, and 41 are difficult to determine. It appears that most ON–OFF clusters also have downward deflections (14–20) reflecting a stronger OFF input as seen in the flash response. While these population averages demonstrate modest success for the present pseudocalcium classification technique, we also found STA diversity within RGC groups that suggest remaining inadequacies in classification. This issue will be addressed in detail in a subsequent study.

Discussion

Our main concern was to classify mouse RGCs to one of 32 proposed RGC types described in the catalog of Baden et al. (2016). In order to match our extracellular spiking activity with their calcium imaging-based clustering data, we transformed RGC spike responses into pseudocalcium traces. Of their 32 groups, 27 were matched by our data. In support of our work in bionic vision, these RGCs were also presented with an electrical noise stimulus (Sekhar et al., 2016). The resultant STAs have been previously shown to

https://doi.org/10.1017/S0952523821000158 Published online by Cambridge University Press

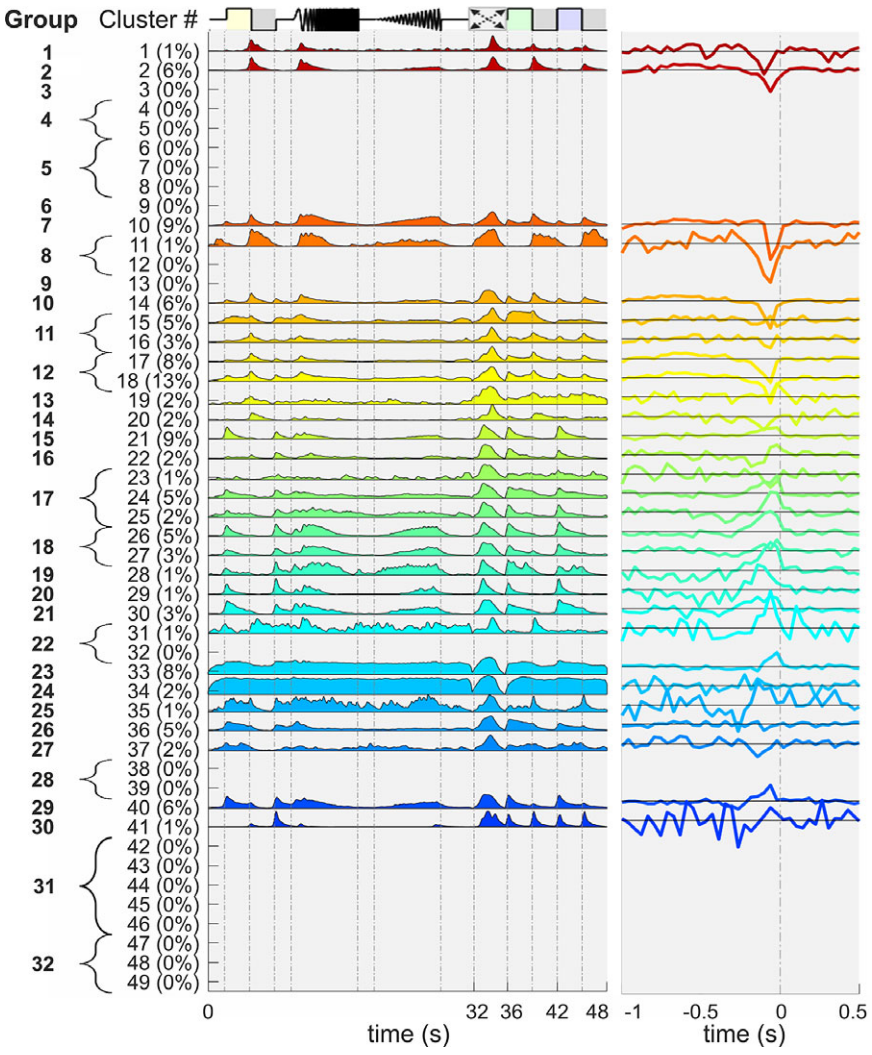


Fig. 4. Response of classified cells to electrical noise stimulus. (*left*) Cluster averages for only the cells with significant electrical STAs, taken from Fig. 3, right. (Order of visual stimuli is as in Fig. 3). (*right*) Electrical STAs averaged across all cells assigned to the cluster. For each STA, horizontal line represents the stimulus mean of −800 mV. Traces above this line indicate that stimuli preceding spikes were on average a higher (less negative) voltage, traces below the line reflect more negative voltages. STA amplitudes were scaled to show detail. Traces to the right of time zero reflect the variation of random noise.

vary with coarsely defined RGC type (Sekhar et al., 2017; Ho et al., 2018). In surveying the STAs of our 27 matched groups, we found some evidence to suggest group-specific filters, however, many groups contained multiple filter shapes. Given known inadequacies in classification, elaborated below, we cannot yet discount the possibility that many RGC groups might possess unique input filters; however, the present results are unable to convincingly support or reject that hypothesis.

On putative RGC type catalogs

Many authors have recently attempted to collect all known and heretofore unknown RGC types into a single visual response classification scheme (Bae et al., 2018; Jouty et al., 2018; Rheaume et al., 2018; Tran et al., 2019). Accordingly, the study of Baden et al. on which we have based our work is no longer the most complete or definitive. Nevertheless, it was one of the first reasonably complete attempts; and so we have anchored the present work on it for better or worse. It is likely that some of the mixed electrical filters reported here may result from incompletely differentiated types in the underlying classification scheme. To resolve the issue, we must refine our methods so that our data can be classified against the most complete schemes available. At present, we find the spike train metrics of Jouty et al. to be quite compelling and although Bae et al. appears to be a remarkably complete classification scheme, it remains unclear how to achieve such classification solely with visual response spike trains. Our group has already moved on to type definitions intrinsic to spike trains on which we will report shortly. Nevertheless, in undertaking this work we were surprised to find few references in the literature to the type of pseudocalcium approach we have taken here—despite its self-evident nature. Likely many others have met with similar disappointment and opted not to share their learned experience. Therefore, in recognizing the utility of so-called negative results, this paper has been submitted to establish such a record.

Subthreshold calcium signals

Although the pseudocalcium method matched our data to most of the RGC groups reported in Baden et al. (2016), it failed to match all

https://doi.org/10.1017/S0952523821000158 Published online by Cambridge University Press

groups. Many of our RGC clusters also had shorter chirp response durations than their reference clusters (e.g., 10 and 29). Consequently, our data failed to match the most sustained clusters (e.g., 3–9, 12–13, 22, 31–32, 38–39, and 42–49). We interpret this to arise from strong subthreshold calcium signals that do not translate into spikes for higher frequencies or lower contrasts. Indeed, calcium signals are known to correspond to subthreshold events like excitatory postsynaptic potentials that are seldom detected in MEA recordings (Nakajima & Baker, 2018). We therefore suspect that many of our cells that should have been matched to sustained groups were misclassified as more transient groups.

Direction selectivity

Direction selectivity is well documented (Briggman et al., 2011); and so it is frustrating that our data failed to yield sufficient multimodality in direction selectivity measures. We attribute this result to the stimulus adaptations that were necessary to support MEA recording. As described in Methods, we replaced the 8 drifting bars that are typically used with 118 bars that drifted along the electrode array to ensure that all eight directions were presented to any possible recording location. Because these drifting bars were seldom centered on a recorded RGC, the ~3 bars of each direction that most directly crossed a cell's receptive field were used—resulting in imperfect response estimates. Additionally, with only five repetitions for any given bar stimulus, it appears that our firing response estimates were too noisy. Nevertheless, remaining visual responses were sufficient to assign cells from our dataset to each of the DS and OS groups.

Alpha cells

One category of RGC type that we often failed to match was alpha cells. In the Baden study, alpha cells were identified based on soma size. Because our MEA recordings did not allow us to measure soma size, we failed to match five of six OFF alpha clusters, leading to two unmatched OFF groups. Nevertheless, we did match data to one OFF and the two ON alpha groups, using only visual responses.

Missing ON cells

A hallmark of the original Baden study was that none of the 49 RGC clusters accounted for more than 5% of the overall RGC population with the vast majority only containing 1 or 2% of the population. In contrast, classification of our data resulted in many clusters receiving no assignments and others receiving well over 5% and up to 16%. This likely is the result of our more transient chirp responses resulting in many ON cells (clusters 3–9) being assigned to ON–OFF clusters (clusters 14–18). This suspected misclassification is understandable considering that the ON clusters of Baden et al. also had significant onset and offset responses (ON–OFF-like behavior) to the drifting bar stimulus.

Notably, the "ON sustained" group 22 (clusters 31 and 32) was largely absent in our classified data; whereas, we found that 17% of our RGCs (110 cells) were assigned to group 38 (clusters 58, 59, and 60)—one of the ON sustained AC groups. In the original Baden et al. study, ACs, like alpha cells, were also reclustered—this time based on immunohistochemistry labeling. Because we cannot fully rule out spiking AC signals from our dataset, we included the AC clusters (50–75) in assigning our RGC data even though recording of extracellular AC spiking responses is expected to be exceedingly rare compared to calcium imaging of AC responses. We suspect, however that these group 38 cells were misclassified and are actually group 22 RGCs. Beyond these, only 14 other RGCs were assigned to AC clusters (50–75).

Spikes versus calcium signals for classification

Both calcium signals and spike trains have their relative advantages and disadvantages for the purposes of classifying RGCs. In common, both methods reflect the stimulus-modulated spiking rate. While calcium signals provide additional information about subthreshold events, spike trains provide more precise timing information. The degree to which information from these sources is redundant *versus* independent, and the degree to which this information can be used in RGC type classification remains to be determined.

Ideally, high-quality calcium recordings simultaneous with MEA recordings would maximize information for high-throughput RGC classification. This would also better connect spike trains with calcium signals. Many labs including ours, however, lack either the resources or expertise to execute such an approach, or are investigating experimental questions that preclude this approach. A worthy goal toward which many are working is to develop methods to infer between calcium and spike train data. Although there is a lack of proper solutions for reconstructing calcium signals from spike traces, many algorithms have been developed for the inverse estimation of spike activity from neuronal calcium imaging. Examples of such approaches include template-matching (Greenberg et al., 2008), deconvolution techniques (Grewe et al., 2010) and approximate Bayesian inference (Deneux et al., 2016). For the inverse problem, inferring calcium data from spike trains has received relatively little discussion in the literature. The present work appears to be one of the relatively few examples where the calcium kernel has been used in the opposite direction to infer calcium traces from known spike trains. Due to limited work on this problem, the two complementary methods of MEA and calcium recording, and their resultant knowledge domains continue to be relatively siloed from one another. We hope that our open discussion of our difficulties in this realm might help others to break through this barrier.

Connecting healthy and blind retinal electrophysiology for bionic vision

Finally, connecting electrical responsiveness data from the healthy mouse retina to the blind retina remains a difficult unresolved problem in our field. Our group has typically taken the approach of working first in the healthy retina to develop new methods because healthy tissue has a significantly higher yield of useful data per animal. That said, we have also performed experiments similar to those described here in intermediate and fully blind mouse retinas. We are pursuing preliminary evidence that electrical response properties themselves may be an effective way to classify RGCs according to visual type in the blind retina. Much more work remains in this area and both the Rathbun and Hosseinzadeh labs are actively expanding their patch clamping abilities to better understand how electrical responses can be used to identify RGC types in the blind retina. Our work will prove useful not only in blind retina research, but in bidirectional bionic vision implants where recordings from the electrode array can be used to map out the "labeled lines" of the underlying cells so that the "correct" visual information is delivered to each cell.

https://doi.org/10.1017/S0952523821000158 Published online by Cambridge University Press

Data availability statement. The data that support the findings of this study are openly available in Zenodo at http://doi.org/10.5281/zenodo.4462320.

Acknowledgments. We thank Prof. Thomas Euler, Prof. Philip Berens, and Master Yannik Bauer for their guidance in understanding the reference paper. This project was built upon the Master's thesis work of Mahdi Sadeghi.

Author contributions. D.L.R. and Z.H. are shared last authors. H.S. and Z.H. performed the experiments. H.S., E.Z., D.L.R., and Z.H. interpreted the results. H.S., D.L.R., and Z.H. designed the study and drafted the manuscript. All authors corrected and approved the final version of the manuscript.

Funding statement. This work was supported by the Deutsche Forschungsgemeinschaft (HO 6221/1-1) to Z.H., by the Bundesministerium für Bildung und Forschung (031a308) to D.L.R., and by the Tistou and Charlotte Kerstan Foundation to Z.H.

Competing interest. The authors have no competing interest to declare.

References

Ayton, L.N., Barnes, N., Dagnelie, G., Fujikado, T., Goetz, G., Hornig, R., Jones, B.W., Muqit, M.M.K., Rathbun, D.L., Stingl, K., Weiland, J.D. & Petoe, M.A. (2020). An update on retinal prostheses. *Clinical Neurophysiology* **131**, 1383–1398.

Baden, T., Berens, P., Franke, K., Román Rosón, M., Bethge, M. & Euler, T. (2016). The functional diversity of retinal ganglion cells in the mouse. *Nature* **529**, 345–350.

Bae, J.A., Mu, S., Kim, J.S., Turner, N.L., Tartavull, I., Kemnitz, N., Jordan, C.S., Norton, A.D., Silversmith, W.M., Prentki, R., Sorek, M., David, C., Jones, D. L., Bland, D., Sterling, A.L.R., Park, J., Briggman, K.L., Seung, H.S. & EYEWIRERS. (2018). Digital museum of retinal ganglion cells with dense anatomy and physiology. *Cell* **173**, 1293–1306.e19.

Barlow, H.B., Hill, R.M. & Levick, W.R. (1964). Retinal ganglion cells responding selectively to direction and speed of image motion in the rabbit. *The Journal of Physiology* **173**, 377–407.

Barlow, H.B. & Levick, W.R. (1965). The mechanism of directionally selective units in rabbit's retina. *The Journal of Physiology* **178**, 477–504.

Boycott, B.B. & Wässle, H. (1974). The morphological types of ganglion cells of the domestic cat's retina. *The Journal of Physiology* **240**, 397–419.

Briggman, K.L., Helmstaedter, M. & Denk, W. (2011). Wiring specificity in the direction-selectivity circuit of the retina. *Nature* **471**, 183–188.

Carcieri, S.M., Jacobs, A.L. & Nirenberg, S. (2003). Classification of retinal ganglion cells: A statistical approach. *Journal of Neurophysiology* **90**, 1704–1713.

Demchinsky, A.M., Shaimov, T.B., Goranskaya, D.N., Moiseeva, I.V., Kuznetsov, D.I., Kuleshov, D.S. & Polikanov, D.V. (2019). The first deaf-blind patient in Russia with Argus II retinal prosthesis system: What he sees and why. *Journal of Neural Engineering* **16**, 025002.

Deneux, T., Kaszas, A., Szalay, G., Katona, G., Lakner, T., Grinvald, A., Rózsa, B. & Vanzetta, I. (2016). Accurate spike estimation from noisy calcium signals for ultrafast three-dimensional imaging of large neuronal populations in vivo. *Nature Communications* **7**, 12190.

Enroth-Cugell, C. & Robson, J.G. (1966). The contrast sensitivity of retinal ganglion cells of the cat. *The Journal of Physiology* **187**, 517–552.

Farrow, K. & Masland, R.H. (2011). Physiological clustering of visual channels in the mouse retina. *Journal of Neurophysiology* **105**, 1516–1530.

Greenberg, D.S., Houweling, A.R. & Kerr, J.N.D. (2008). Population imaging of ongoing neuronal activity in the visual cortex of awake rats. *Nature Neuroscience* **11**, 749–751.

Grewe, B.F., Langer, D., Kasper, H., Kampa, B.M. & Helmchen, F. (2010). High-speed in vivo calcium imaging reveals neuronal network activity with near-millisecond precision. *Nature Methods* **7**, 399–405.

Grienberger, C. & Konnerth, A. (2012). Imaging calcium in neurons. *Neuron* **73**, 862–885.

Ho, E., Smith, R., Goetz, G., Lei, X., Galambos, L., Kamins, T.I., Harris, J., Mathieson, K., Palanker, D. & Sher, A. (2018). Spatiotemporal characteristics of retinal response to network-mediated photovoltaic stimulation. *Journal of Neurophysiology* **119**, 389–400.

Hosseinzadeh, Z., Jalligampala, A., Zrenner, E. & Rathbun, D.L. (2017). The spatial extent of epiretinal electrical stimulation in the healthy mouse retina. *Neurosignals* **25**, 15–25.

Hosseinzadeh, Z., Rathbun, D.L. & Zrenner, E. (2019). Selective activation of ON and OFF RGC input in mouse retina stimulated. *Investigative Ophthalmology & Visual Science* **60**, 4989.

Jalligampala, A., Sekhar, S., Zrenner, E. & Rathbun, D.L. (2017). Optimal voltage stimulation parameters for network-mediated responses in wild type and rd10 mouse retinal ganglion cells. *Journal of Neural Engineering* **14**, 026004.

Jouty, J., Hilgen, G., Sernagor, E. & Hennig, M.H. (2018). Non-parametric physiological classification of retinal ganglion cells in the mouse retina. *Frontiers in Cellular Neuroscience* **12**, 481.

Kuffler, S.W. (1953). Discharge patterns and functional organization of mammalian retina. *Journal of Neurophysiology* **16**, 37–68.

Nakajima, R. & Baker, B.J. (2018). Mapping of excitatory and inhibitory postsynaptic potentials of neuronal populations in hippocampal slices using the GEVI, ArcLight. *Journal of Physics D: Applied Physics* **51**, 504003.

Perry, V.H. & Cowey, A. (1984). Retinal ganglion cells that project to the superior colliculus and pretectum in the macaque monkey. *Neuroscience* **12**, 1125–1137.

Rathbun, D.L., Ghorbani, N., Shabani, H., Zrenner, E. & Hosseinzadeh, Z. (2018). Spike-triggered average electrical stimuli as input filters for bionic vision-a perspective. *Journal of Neural Engineering* **15**, 063002.

Rheaume, B.A., Jereen, A., Bolisetty, M., Sajid, M.S., Yang, Y., Renna, K., Sun, L., Robson, P. & Trakhtenberg, E.F. (2018). Single cell transcriptome profiling of retinal ganglion cells identifies cellular subtypes. *Nature Communications* **9**, 2759.

Sekhar, S., Jalligampala, A., Zrenner, E. & Rathbun, D.L. (2016). Tickling the retina: Integration of subthreshold electrical pulses can activate retinal neurons. *Journal of Neural Engineering* **13**, 046004.

Sekhar, S., Jalligampala, A., Zrenner, E. & Rathbun, D.L. (2017). Correspondence between visual and electrical input filters of ON and OFF mouse retinal ganglion cells. *Journal of Neural Engineering* **14**, 046017.

Shew, W.L., Bellay, T. & Plenz, D. (2010). Simultaneous multi-electrode array recording and two-photon calcium imaging of neural activity. *Journal of Neuroscience Methods* **192**, 75–82.

Tran, N.M., Shekhar, K., Whitney, I.E., Jacobi, A., Benhar, I., Hong, G., Yan, W., Adiconis, X., Arnold, M.E., Lee, J.M., Levin, J.Z., Lin, D., Wang, C., Lieber, C. M., Regev, A., He, Z. & Sanes, J.R. (2019). Single-cell profiles of retinal ganglion cells differing in resilience to injury reveal neuroprotective genes. *Neuron* **104**, 1039–1055.e12.

Wässle, H. (2004). Parallel processing in the mammalian retina. *Nature Reviews. Neuroscience* **5**, 747–757.

Williamson, R.S., Sahani, M. & Pillow, J.W. (2015). The equivalence of information-theoretic and likelihood-based methods for neural dimensionality reduction. *PLoS Computational Biology* **11**, e1004141.

Zrenner, E. (2002). Will retinal implants restore vision? *Science* **295**, 1022–1025.

https://doi.org/10.1017/S0952523821000158 Published online by Cambridge University Press